Research Article

Histochemistry of microinfarcts in the mouse brain after injection of fluorescent microspheres into the common carotid artery

https://doi.org/10.4103/1673-5374.322470

Date of submission: January 25, 2021

Date of decision: March 8, 2021

Date of acceptance: July 2, 2021

Date of web publication: August 30, 2021

Yi Shen[1, #], Ming-Jiang Yao[2, 3, #], Yu-Xin Su[1], Dong-Sheng Xu[1], Jia Wang[1], Guang-Rui Wang[2, 3], Jing-Jing Cui[1], Jian-Liang Zhang[1], Wan-Zhu Bai[1, *]

Graphical Abstract *Histochemical changes following cerebral microinfarcts induced by fluorescent microspheres*

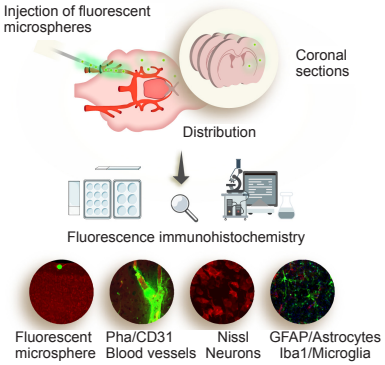

Abstract

The mouse model of multiple cerebral infarctions, established by injecting fluorescent microspheres into the common carotid artery, is a recent development in animal models of cerebral ischemia. To investigate its effectiveness, mouse models of cerebral infarction were created by injecting fluorescent microspheres, 45–53 μm in diameter, into the common carotid artery. Six hours after modeling, fluorescent microspheres were observed directly through a fluorescence stereomicroscope, both on the brain surface and in brain sections. Changes in blood vessels, neurons and glial cells associated with microinfarcts were examined using fluorescence histochemistry and immunohistochemistry. The microspheres were distributed mainly in the cerebral cortex, striatum and hippocampus ipsilateral to the side of injection. Microinfarcts were found in the brain regions where the fluorescent microspheres were present. Here the lodged microspheres induced vascular and neuronal injury and the activation of astroglia and microglia. These histopathological changes indicate that this animal model of multiple cerebral infarctions effectively simulates the changes of various cell types observed in multifocal microinfarcts. This model is an effective, additional tool to study the pathogenesis of ischemic stroke and could be used to evaluate therapeutic interventions. This study was approved by the Animal Ethics Committee of the Institute of Acupuncture and Moxibustion, China Academy of Chinese Medical Sciences (approval No. D2021-03-16-1) on March 16, 2021.

Key Words: astrocytes; blood-brain barrier; common carotid artery; fluorescent microsphere; histochemistry; ischemia; microglia; microinfarcts; neuron; neurovascular unit; stroke

Chinese Library Classification No. R446; R741; R363

Introduction

Ischemic stroke is caused by blockage of blood vessels in the brain leading to high levels of disability and mortality worldwide. Although our understanding of the structural characteristics of ischemic stroke has progressed, its pathological impact remains poorly understood (Moskowitz et al., 2010; Brundel et al., 2012; Smith et al., 2012; van Veluw et al., 2017; Shindo et al., 2020). Most of the research on the histopathological changes in ischemic stroke has been obtained from ischemic models. The ischemic model produced by intravascular injection of fluorescent microspheres into one side of common carotid artery (CCA) has recently been the preferred choice for the histochemical examination of the cellular changes in microinfarcts (Bere et al., 2014; Silasi et al., 2015; Tsukada et al., 2018; Balbi et al., 2019).

The breakdown of the blood-brain barrier (BBB) or the dysfunction of neurovascular unit (NVU) are considered the prime pathological characteristics of ischemic stroke (del

[1]Institute of Acupuncture and Moxibustion, China Academy of Chinese Medical Sciences, Beijing, China; [2]Institute of Basic Medical Sciences, Xiyuan Hospital of China Academy of Chinese Medical Sciences, Beijing, China; [3]Beijing Key Laboratory of Pharmacology of Chinese Materia Medica, Beijing, China

*Correspondence to: Wan-Zhu Bai, PhD, wanzhubaisy@hotmail.com.

https://orcid.org/0000-0001-6285-7788 (Wan-Zhu Bai)

#Both authors contributed equally to the work.

Funding: *This study was supported by the Project of National Key R&D Program of China, No. 2019YFC1709103 (to WZB); and the National Natural Science Foundation of China, Nos. 81774211 (to WZB), 81873040 (to MJY), 81774432 (to JJC), 81801561 (to DSX), 82004492 (to JW).*

How to cite this article: *Shen Y, Yao MJ, Su YX, Xu DS, Wang J, Wang GR, Cui JJ, Zhang JL, Bai WZ (2022) Histochemistry of microinfarcts in the mouse brain after injection of fluorescent microspheres into the common carotid artery. Neural Regen Res 17(4):832-837.*

Zoppo, 2009, 2010; Barakat and Redzic, 2016; Iadecola, 2017; Caffrey et al., 2021; Ye et al., 2021), therefore it is reasonable to examine the alteration of the cellular components of the BBB or NVU with a vascular blockage model (Abbott et al., 2006; Prakash and Carmichael, 2015; Jiang et al., 2018; Freitas-Andrade et al., 2020). In this study, we focused on vascular cells, neurons, astrocytes and microglia in the regions of the microinfarcts. We generated a mouse model of cerebral microinfarcts by injecting fluorescent microspheres, 45–53 μm in diameter, into one side of the CCA. Fluorescent histochemistry and immunohistochemistry were carried out to analyze the multicellular changes associated with the ensuing microinfarcts. Phalloidin and platelet endothelial cell adhesion molecule-1 (CD31) were selected to label vascular smooth muscle cells and vascular endothelial cells, as previously reported (Woodfin et al., 2007; Chazotte, 2010; Chistiakov et al., 2016; Wang et al., 2020). Nissl and caspase 3 were used to evaluate neuronal degeneration. Glial fibrillary acidic protein (GFAP) and ionized calcium binding adapter molecule 1 (Iba1) were used as measures of astroglial and microglial activation, respectively (Abbott et al., 2006; Barakat and Redzic, 2016; Jiang et al., 2018). All these techniques enable assessment of how the various cells change in response to the cerebral microinfarcts.

Materials and Methods

This study was approved by the Animal Ethics Committee of the Institute of Acupuncture and Moxibustion, China Academy of Chinese Medical Sciences (approval No. D2021-03-16-1) on March 16 2021 and was carried out in accordance with the National Institutes of Health Guide for the Care and Use of Laboratory Animals (National Academy Press, Washington, DC, USA).

Animals

Eight adult male C57BL/6 mice (6–8 weeks old, weighing 20–25 g) were provided by the Institute of Laboratory Animal Sciences, Chinese Academy of Medical Sciences, China (license No. SCXK (Jing) 2019-0010) for use in this study. All animals were housed in a 12-hour light/dark cycle with controlled temperature and humidity and allowed free access to food and water.

Fluorescent microspheres

Fluorescent polyethylene microspheres made of polystyrene in a series of sizes were provided by Cospheric LLC (Santa Barbara, CA, USA). The diameter of the right internal carotid artery is 121.29 ± 12.79 μm in mice (Qian et al., 2018) and we selected microspheres with 45–53 μm in diameter (UVPMS-BY2-1.00, 16,223,536 U/g), for intravascular injection as previously reported (Bere et al., 2014).

Surgical procedure for microsphere injection

In all experiments and surgical approaches, anesthesia was induced by intraperitoneal injection of pentobarbital sodium (50 mg/kg, Cat# 020402, Beijing Chemical Reagent Research Institute Co., Ltd., Beijing, China). Intravascular injection was performed as described previously (Bere et al., 2014; Silasi et al., 2015). In brief, a cervical incision was made to insert a polyethylene tube (PE-10 medical tube; Imamura Co. Ltd., Tokyo, Japan) into the right side of the CCA. In this procedure the proximal sides of the CCA and the external carotid artery were ligated with surgical silk, but not the pterygopalatine artery, while the polyethylene tube was inserted into the distal portion of the CCA. A total of 100 μL of 1000 unit of microspheres (~616 μg/mL) suspended in 5% Dextran T-40 (Cat# D8250, Solarbio Science & Technology Co., Ltd., Beijing, China) and then injected into each experimental animal through the polyethylene tube (n = 6). Vehicle controls received 100 μL 5% Dextran T-40 (n = 2). After injection, the polyethylene tube was withdrawn and the distal portion of the CCA was ligated simultaneously with surgical silk. The mice were kept warm with a hot blanket until they recovered from the anesthetic postoperatively.

Perfusions and sections

Six hours after the operation all mice were anesthetized again by intraperitoneal injection of pentobarbital sodium (50 mg/kg) and transcardially perfused with saline followed with 4% paraformaldehyde in 0.1 M phosphate buffer (PB, pH 7.4). The brain was dissected out and post-fixed in 4% paraformaldehyde in PB for 2 hours, then cryoprotected overnight in 25% sucrose. Fluorescent microspheres on the cerebral cortex were observed over the brain surface (**Figure 1**) using a fluorescence stereomicroscope (MVX10; Olympus, Tokyo, Japan). After examining the whole brain, each was cut into 80 μm-thick coronal sections with a freezing microtome (Thermo, Microm International GmbH, Walldorf, Germany) and the sections were collected in order in a six-hole Petri dish with 0.1 M PB (pH 7.4). The sites of lodged microspheres and microinfarcts in the brain were assessed according to a previous study (Paxinos and Franklin, 2001).

Fluorescent histochemical and immunohistochemical examinations

Fluorescent histochemical and immunohistochemical examinations were performed in four parts: (1) Nissl staining, (2) phalloidin + CD31, (3) Nissl staining + caspase 3, and (4) GFAP + Iba1 + 4′,6-diamidino-2-phenylindole (DAPI). Every sixth sections of the brain were used in each examination. For Nissl staining, the brain sections were directly stained by NeuroTrace™ 530/615 Red Fluorescent Nissl Stain (1:2000, Cat# N21482, Thermo Fisher, Waltham, MA, USA) in 0.1 M PB containing 1% Triton X-100 for 2 hours at room temperature. In phalloidin + CD31, Nissl staining + caspase 3, and GFAP + Iba1 + DAPI examinations, the sections were incubated in blocking solution containing 3% normal donkey serum (Cat# 017-000-121, Jackson ImmunoResearch, West Grove, PA, USA) and 1% Triton X-100 in 0.1 M PB (pH 7.4) for 0.5 hours at room temperature. The sections in these three parts were then incubated separately with primary antibodies: mouse anti-CD31 (1:1000, Cat# ab24590, Abcam, Cambridge, UK), rabbit anti-cleaved Caspase-3 (Asp175) (1:500, Cat# 9661, Cell Signaling, Danvers, MA, USA), or mouse anti-GFAP (1:1000, Cat# G3893, Sigma, St. Louis, MO, USA) and rabbit anti-Iba1 (1:1000, Abcam, Cat# ab178847) solution at 4°C overnight.

On the next day, the samples were washed in 0.1 M PB (pH 7.4) and incubated with the secondary antibodies and bio-markers corresponding to the groups described above: including donkey anti-mouse Alexa Fluor 488 (1:500, Thermo Fisher, Cat# A21202) and Alexa Fluor 568 phalloidin (1:1000, Thermo Fisher, Cat# A12380) for part (2), donkey anti-rabbit Alexa Fluor 594 (1:500, Thermo Fisher, Cat# A21207) and NeuroTrace™ 500/525 Green Fluorescent Nissl Stain (1:2000, Thermo Fisher, Cat# N21480) for part (3), donkey anti-mouse Alexa Fluor 594 (1:500, Thermo Fisher, Cat# A21203), donkey anti-rabbit Alexa Fluor 488 (1:500, Thermo Fisher, Cat# A21206), and DAPI (1:50,000, Thermo Fisher, Cat# D3571) for part (4). All samples were incubated at room temperature for 1.5 hours. After staining, all sections were washed thoroughly with 0.1 M PB (pH 7.4) and mounted on a SuperFrost Plus microscope slide (Thermo Fisher). The samples were sealed with a coverslip in 50% glycerin before microscopic observation. The remaining sections, from each of the four groups, were directly mounted on the SuperFfrost Plus microscope slide to observe the distribution of fluorescent microspheres in the brain.

The samples were scanned with VS120 Virtual Slide System

(Olympus), in which the representative regions were selected for further view and recording with a confocal imaging system (FV1200, Olympus). All images were analyzed using the Olympus Image Processing Software and processed using Adobe Photoshop CS5 (Adobe Systems, San Jose, CA, USA) and Adobe Illustration CS5 (Adobe Systems).

Statistical analysis

All brain sections of the six experimental mice were counted for microsphere distribution. Results are presented as the mean ± standard error of mean (SEM) with SAS version 9.4 (SAS Institute Inc., Cary, NC, USA). The Kruskal-Wallis test was used to evaluate the distribution of fluorescent microspheres in different regions. The difference was considered statistically significant when $P < 0.05$.

Results

Distribution of fluorescent microspheres and microinfarcts

Six hours after intracarotid injection, the fluorescent microspheres were directly observed on the brain surface under the fluorescence stereomicroscope (**Figure 1B**). Additionally, the distribution of fluorescent microspheres was further mapped in the coronal sections of the brain (**Figure 1C**). Microspheres were located in the arterioles, predominately in the cortex but also in the striatum, thalamus, hippocampus and other regions in the cerebral hemisphere ipsilateral to the side of injection (**Figures 1–4**). Microinfarcts were detected in the tissue near where the microspheres lodged in the occluded arterioles or their downstream branches (**Figures 2–4**). Corresponding to the locations of microspheres in the brain, the microinfarcts were scattered in the cortex, striatum, thalamus, hippocampus and other regions. In the cortex, microinfarcts were found in typical wedge shape or column following the lodged microspheres in the penetrating arteriole at the pial surface (**Figures 2–4**). Microinfarcts in other cerebral regions varied in size and shape (**Figures 2–4**). A similar pattern of the distribution of fluorescent microspheres and microinfarcts was found in each microinfarct modelled mouse.

Changes in vascular integrity

The vascular integrity in the regions of microinfarcts was evaluated with phalloidin and CD31 (**Figure 2**). In control cases, phalloidin was expressed on the cerebral arterioles and their downstream branches, while CD31 was mainly present on the capillaries (**Figure 2A** and **C**). However, when the blood vessels were blocked with microspheres, expression of phalloidin followed the lodged microspheres and was found on the collapsed arterioles (**Figure 2B** and **D**). However, CD31 presented not only markedly on the capillaries but also at the location of the blocked blood vessels (**Figure 2**).

Neuronal degeneration and distribution

Neuronal alteration was examined using fluorescent Nissl and caspase 3 histological staining. Compared with the vehicle control, neuronal atrophy or cell loss was clearly demonstrated with Nissl labeling in the regions of microinfarcts (**Figure 3**). Cortical neurons in the layer 5 were typically pyramidal and distributed regularly in the vehicle controls (**Figure 3**), however, the cortical neurons in the region of microinfarcts were shrunken and their distribution was disorganized (**Figure 3**). Caspase 3 was expressed more strongly in the region of microinfarcts than that in the control case (**Figure 3**).

Astroglial and microglial activation

Astroglial and microglial activation was assessed with glial fibrillary acidic protein (GFAP) and Iba1 staining, respectively. In the vehicle controls, astrocytes and microglia presented with delicate cellular processes from their cell bodies and were observed throughout the brain tissue (**Figure 4**). When they were activated by the lodged microspheres, astrocytes gathered in the region of microinfarcts or along the wall of blocked vessels, presenting with thicker cellular processes (**Figure 4**). The microglia changed their form with enlarged cell bodies and short processes and, though scattered in the region of microinfarcts, accumulated particularly in peri-infarct regions (**Figure 4**).

Discussion

In this study, we described the pathological properties of multifocal microinfarcts in the mouse brain induced by the intracarotid injection of fluorescent microspheres. Taking advantage of this experimental model, our results provide histochemical views of the multicellular changes in the regions of cerebral microinfarcts at an early stage (**Figure 5**). This model of ischemic stroke may be beneficial in understanding the underlying mechanisms of multifocal microinfarcts and has the potential to assess novel therapeutic interventions of ischemic stroke.

Technological consideration

Various animal models have been used to investigate ischemic stroke, such as middle cerebral artery occlusion and laser-induced occlusion of penetrating arterioles (Nishimura et al., 2010; Shih et al., 2013, 2015; Taylor and Sansing, 2013; Zhang et al., 2015; Shah et al., 2019). Although the middle cerebral artery occlusion model has been widely used to investigate ischemic stroke, it usually blocks the main trunk of the middle cerebral artery, leading to a large area of cerebral infarction (Shih et al., 2018; Shah et al., 2019). Laser treatment can induce microinfarcts at the brain surface through exquisitely controlling the location and timing of their onset, but it is limited to the surface of cerebral cortex (Shih et al., 2013; Taylor and Sansing, 2013; Zhang et al., 2015). Intracarotid injection of microspheres may complement the experimental models by mimicking the multifocal microinfarcts of ischemic stroke (Bere et al., 2014; Silasi et al., 2015; Tsukada et al., 2018; Balbi et al., 2019).

In the intracarotid injection of microspheres experimental model the microspheres tend to distribute in the hemisphere ipsilateral to the injection site, despite the blood supply of both cerebral hemispheres coming from the bilateral common carotid arteries via the circle of Willis. One possible explanation is that the injection and the ligation were carried out on the same side of CCA. Under these conditions, the blood supply from the contralateral CCA may dynamically prevent the entering of microspheres. This result is consistent with a previous study (Tsukada et al., 2018). In addition, the distribution of microspheres is determined by the diameter of microspheres themselves (Rapp et al., 2003, 2008; Reeson et al., 2018; Tsukada et al., 2018). This corresponds to the correlation between the number of microinfarcts and the diameter of the blood vessels to be blocked in the cerebral regions (Miyake et al., 1993; Bere et al., 2014; Silasi et al., 2015; Balbi et al., 2019).

Since rather large-sized microspheres were used in the present study, they induced the blockage of larger diameter blood vessels, mostly branching from the middle cerebral artery, causing fewer infarcts but over a larger area. In comparison, infarcts induced by small-sized microspheres were limited to a smaller area but occurred in more numerous regions (Silasi et al., 2015). Although a similar model was successfully used in a previous study, only functionally multimodal imaging of the cerebral blood flow from the brain surface was examined (Bere et al., 2014). Importantly, our study additionally demonstrated histochemically the multicellular alterations after the multifocal microinfarcts.

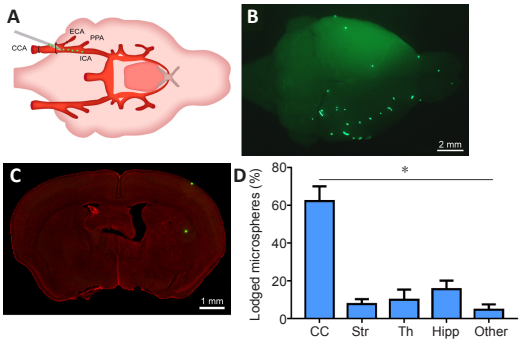

Figure 1 | **Injection and distribution of fluorescent microspheres.**
(A) An illustration for the injection of fluorescent microspheres into the right side of the common carotid artery (CCA) of mice. (B) A representative photograph from the brain surface of mouse under the fluorescence stereomicroscope showing a typical distribution of fluorescent microspheres (green dots) lodged in blood vessels of the cerebral cortex. (C) A representative photograph from the coronal section of mouse brain with fluorescent Nissl staining showing the lodged microspheres (green dots) on the cortical surface and in the striatum. Scale bars: 2 mm in B, 1 mm in C. (D) The distributional percentage of microspheres in the different regions including the cerebral cortex (CC), striatum (Str), thalamus (Th), hippocampus (Hipp), and other regions. Data are expressed as mean ± SEM (n = 6) and were analyzed by Kruskal-Wallis test. *P < 0.05. ECA: External carotid artery; ICA: internal carotid artery; PPA: pterygopalatine artery.

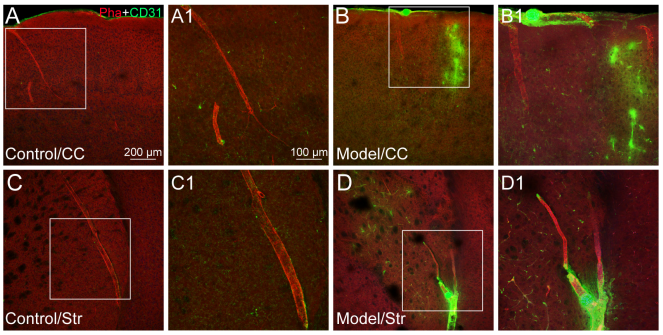

Figure 2 | **The vascular alteration induced by fluorescent microspheres.**
(A–D) The representative photographs from the cerebral cortex (CC; A and B) and striatum (Str; C and D), showing the histological features of phalloidin (Pha, red, Alexa Fluor 568)- and CD31 (green, Alexa Fluor 488)-labeled blood vessels in the cases of control (A and C) and experimental model (B and D). (A1–D1) Magnified photographs from the box-indicated regions in panels A–D showing Pha- and CD31-labeled blood vessels in detail, respectively. CD31 labeling expressed more strongly in the regions of microinfarct than that of control. The vascular alteration in all model mice presented in a similar pattern (n = 6). Green dots in panels B/B1 (upper edge) and D/D1 (lower edge) are the lodged fluorescent microspheres. Scale bars: 200 μm in A–D, 100 μm in A1–D1.

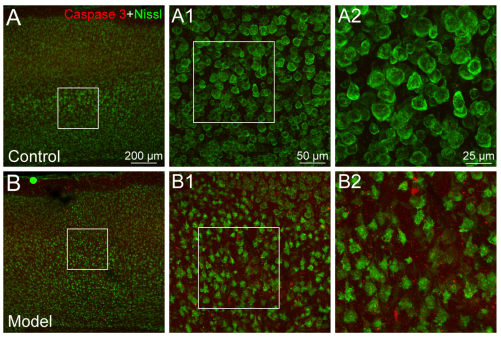

Figure 3 | **The neuronal degeneration in the region of microinfarcts.**
(A, B) The representative photographs from the cerebral cortex showing the Nissl (green, NeuroTrace™ 500/525) and caspase 3 (red, Alexa Fluor 594)-labeling in the cases of control (A) and experimental model (B). (A1, B1) Magnified photographs from the box-indicated regions in panels A and B showing Nissl and caspase 3 labeling in detail, respectively. (A2, B2) Higher magnified photographs from panels A1 and B1. In contrast to the control, neurons are shrunken and caspase 3 labeling is expressed more strongly in the region of microinfarct. The neuronal degeneration in all the model mice presented a similar pattern (n = 6). Green dot in panel B is a lodged fluorescent microsphere on the pial surface. Scale bars: 200 μm in A and B, 50 μm in A1 and B1, 25 μm in A2 and B2.

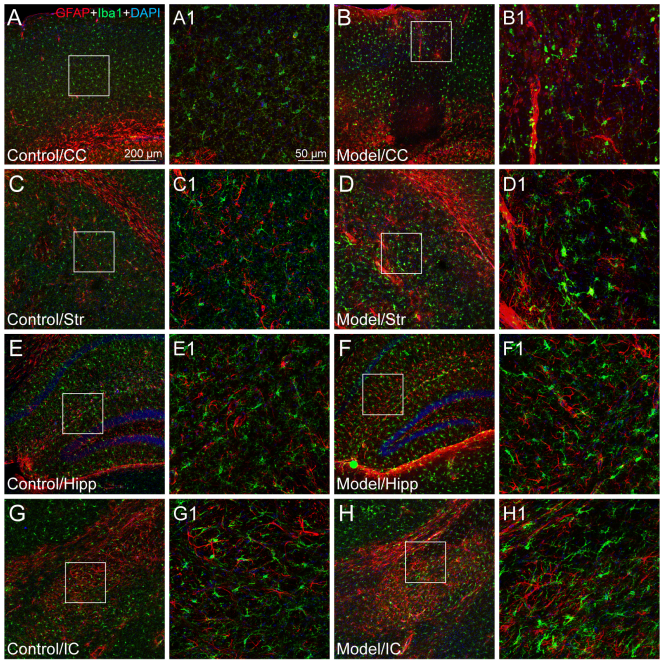

Figure 4 | **The astroglial and microglial activation in different regions of microinfarcts.**
(A–H) The representative photographs from the cerebral cortex (CC, A and B), striatum (Str, C and D), hippocampus (Hipp, E and F), and internal capsule (IC, G and H) showing the glial fibrillary acidic protein (GFAP, red, Alexa Fluor 594)-labeled astrocytes and ionized calcium binding adapter molecule 1 (Iba1, green, Alexa Fluor 488)-labeled microglia in the cases of control (A, C, E, G) and experimental model (B, D, F, H). (A1–H1) Magnified photographs from the box-indicated regions in panels A–H showing the GFAP- and Iba1-labeling in detail. In the controls, the resting astrocytes and microglia were delicate in form and were distributed evenly in the different regions. In contrast, active astrocytes and microglia in the region of microinfarcts presented with enlarged cell bodies and the thicker cellular processes gathering around the wall of blocked vessels or scattered within the region of the microinfarcts. The astroglial and microglial activation in all model mice presented with the similar pattern (n = 6). The green dot in panel F is a lodged fluorescent microsphere near the hippocampus. Scale bars: 200 μm in A–H, 50 μm in A1–H1. DAPI: 4′,6-Diamidino-2-phenylindole.

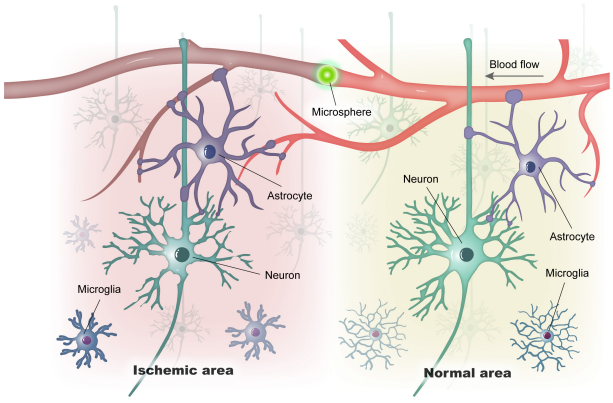

Figure 5 | **A simplified illustration of vascular and cellular alteration of microinfarct induced by a lodged fluorescent microsphere in the cerebral blood vessel.**
In contrast to the normal area, the pathological alteration in the ischemic area includes the vascular blocking, neuronal degeneration, and astroglial/microglial activation.

Technological and design limitations

Despite the technological advantage that fluorescent microspheres are more easily identified in the blocked vessels in the brain, it should be noted here that these microspheres are made from polystyrene that can be dissolved by xylene. Therefore, conventional staining methods involving treatment with xylene cannot be used on brain sections with lodged microspheres. Instead, fluorescent histochemical or fluorescent immunohistochemical staining is recommended. In addition, it should be emphasized that the pathological changes that we observed on the microinfarcts came from only one time point, therefore our results are neither comprehensive nor do they reflect the complicated cascade of cellular changes. Further research is required to fully elucidate the dynamic changes following microinfarcts. This preliminary study has clearly demonstrated histopathologically the vascular, neuronal and glial alterations in all mice with the microinfarct model compared with those of vehicle controls, suggesting this is an effective model for microinfarcts. The limited number of animals focused our observations on the morphological changes. A larger study would be required for quantitative histological and statistical analysis. Finally, it should be noted that gender differences are well known in ischemic stroke (Ahnstedt et al., 2016). Our study used only male mice therefore female mice should be included in future studies using this model.

Vascular, neuronal, and glial alteration associated with microinfarcts

The fluorescent microbead ischemia model allowed us to analyze the multicellular alteration associated with multifocal microinfarcts at the early stage of ischemia. As with other types of ischemic stroke (del Zoppo, 2009, 2010; Barakat and Redzic, 2016; Iadecola, 2017; Freitas-Andrade et al., 2020), the breakdown of BBB and NVU is also thought to be the major features of the present model. Here, we demonstrated that the lodged microspheres greatly altered vascular integrity, resulting in vascular and neuronal injury, as well as astroglial and microglial activation in the insulted regions.

According to the expression of phalloidin and CD31 labeling, the smooth muscle cells and endothelial cells of the arterioles were obviously disrupted in the regions of microinfarcts. As the first-line defense to ischemia and hypoxia, endothelial cells play a critical role in maintaining the homeostasis of the brain under physiological conditions. However, endothelial dysfunction can increase BBB permeability and subsequently lead to lesioning of the brain parenchyma (Jiang et al., 2018; Mustapha et al., 2019).

In the present study, phalloidin was chosen as a suitable biomarker for labeling the cerebral arteries under both normal and pathological conditions. In contrast, CD31 labelled the capillaries in the regions of microinfarcts more strongly than those of controls. It is not yet clear whether this phenomenon is correlated with angiogenesis (Woodfin et al., 2007; Chazotte, 2010; Chistiakov et al., 2016; Alarcon-Martinez et al., 2018; Wang et al., 2020). In parallel to the vascular injury, neuronal degeneration was observed in focal regions of the microinfarcts six hours after the ischemia modelling. It reflects the neuronal and vascular vulnerability within the vascular territory-at-risk, indicating that vascular disorder with neurological consequences is an acute event for ischemic stroke (Rapp et al., 2000; del Zoppo, 2010; Kim et al., 2016).

Histological studies show that astrocytes are ideally positioned to conduct information in a bidirectional manner between neurons and blood vessels (Zonta et al., 2003; Takano et al., 2006; Mishra et al., 2016; Jiang et al., 2018). Our results clearly showed that astroglial activation was involved in the pathological alteration of blood vessels and neurons. Since activated astrocytes are mainly found in the region of microinfarcts and along the walls of blocked vessels, it implies that astrocytes could form a barrier to confine the spread of the lesion, although it may also result in the formation of glial scar to impede neurogenesis and neurological recovery (Jiang et al., 2018).

In contrast to astrocytes, microglia as the resident immune cells can also actively respond to the ischemic injury (Hanisch and Kettenmann, 2007; Kettenmann et al., 2011; Tremblay et al., 2011). In the present model, although most of the activated microglia did not exhibit amoeboid morphology, they had enlarged cell bodies and short processes, an indication of activation against microinfarcts. However, the precise role of activated microglia during the ischemic stroke, whether detrimental or beneficial, is still poorly understood (Hu et al., 2012; Patel et al., 2013; Mallucci et al., 2015; Jiang et al., 2018).

Currently, our understanding of acute multicellular alteration to ischemic stroke is incomplete (Mustapha et al., 2019). As integral parts of the BBB or NVU, endothelial cells, neurons and glial cells are interconnected and interact, contributing to brain homeostasis under the physiological condition (Shih et al., 2006; Attwell et al., 2010; Andreone et al., 2015; Iadecola, 2017). However, this homeostasis is disturbed by ischemic stroke leading to rapid cellular changes (Prakash and Carmichael, 2015; Jiang et al., 2018; Freitas-Andrade et al., 2020). Although the present work only focuses on histopathological changes, we hope that this model will open a new technical window to understand the multicellular alteration associated with multifocal microinfarcts.

In summary, we have established an experimental model of ischemic stroke using fluorescent microspheres, which simulated multifocal microinfarcts causing multicellular changes. This model is a valid tool for investigating the underlying mechanisms of ischemic stroke and assessing its therapeutic intervention. Our histopathological findings also suggest that therapeutic intervention would be most effective for patients if carried out at the early stage of ischemic stroke.

Author contributions: *Study conception and design: YS, MJY, WZB; model preparation: YS, MJY, YXS, GRW; histochemical staining and sample observation: YS, JW, JJC; data analysis and figure preparation: DSX, JLZ; manuscript drafting: YS, WZB. All authors approved the final manuscript.*
Conflicts of interest: *The authors declare no conflicts of interest.*
Financial support: *This study was supported by the Project of National Key R&D Program of China, No. 2019YFC1709103 (to WZB); and the National Natural Science Foundation of China, Nos. 81774211 (to WZB), 81873040 (to MJY), 81774432 (to JJC), 81801561 (to DSX), 82004492 (to JW). The funding sources had no role in study conception and design, data analysis or interpretation, paper writing or deciding to submit this paper for publication.*
Institutional review board statement: *This study was approved by the Animals Ethics Committee of the Institute of Acupuncture and Moxibustion, China Academy of Chinese Medical Sciences (approval No. D2021-03-16-1) on March 16, 2021.*

Data sharing statement: *Datasets analyzed during the current study available from the corresponding author on reasonable request.*
Plagiarism check: *Checked twice by iThenticate.*
Peer review: *Externally peer reviewed.*

References

Abbott NJ, Rönnbäck L, Hansson E (2006) Astrocyte-endothelial interactions at the blood-brain barrier. Nat Rev Neurosci 7:41-53.

Ahnstedt H, McCullough LD, Cipolla MJ (2016) The importance of considering sex differences in translational stroke research. Transl Stroke Res 7:261-273.

Alarcon-Martinez L, Yilmaz-Ozcan S, Yemisci M, Schallek J, Kılıç K, Can A, Di Polo A, Dalkara T (2018) Capillary pericytes express α-smooth muscle actin, which requires prevention of filamentous-actin depolymerization for detection. Elife 7:e34861.

Andreone BJ, Lacoste B, Gu C (2015) Neuronal and vascular interactions. Annu Rev Neurosci 38:25-46.

Attwell D, Buchan AM, Charpak S, Lauritzen M, Macvicar BA, Newman EA (2010) Glial and neuronal control of brain blood flow. Nature 468:232-243.

Balbi M, Vanni MP, Vega MJ, Silasi G, Sekino Y, Boyd JD, LeDue JM, Murphy TH (2019) Longitudinal monitoring of mesoscopic cortical activity in a mouse model of microinfarcts reveals dissociations with behavioral and motor function. J Cereb Blood Flow Metab 39:1486-1500.

Barakat R, Redzic Z (2016) The role of activated microglia and resident macrophages in the neurovascular unit during cerebral ischemia: is the jury still out? Med Princ Pract 25 Suppl 1:3-14.

Bere Z, Obrenovitch TP, Kozák G, Bari F, Farkas E (2014) Imaging reveals the focal area of spreading depolarizations and a variety of hemodynamic responses in a rat microembolic stroke model. J Cereb Blood Flow Metab 34:1695-1705.

Brundel M, de Bresser J, van Dillen JJ, Kappelle LJ, Biessels GJ (2012) Cerebral microinfarcts: a systematic review of neuropathological studies. J Cereb Blood Flow Metab 32:425-436.

Caffrey TM, Button EB, Robert J (2021) Toward three-dimensional in vitro models to study neurovascular unit functions in health and disease. Neural Regen Res 16:2132-2140.

Chazotte B (2010) Labeling cytoskeletal F-actin with rhodamine phalloidin or fluorescein phalloidin for imaging. Cold Spring Harb Protoc 2010:pdb.prot4947.

Chistiakov DA, Orekhov AN, Bobryshev YV (2016) Endothelial PECAM-1 and its function in vascular physiology and atherogenic pathology. Exp Mol Pathol 100:409-415.

del Zoppo GJ (2009) Inflammation and the neurovascular unit in the setting of focal cerebral ischemia. Neuroscience 158:972-982.

del Zoppo GJ (2010) The neurovascular unit in the setting of stroke. J Intern Med 267:156-171.

Freitas-Andrade M, Raman-Nair J, Lacoste B (2020) Structural and Functional Remodeling of the Brain Vasculature Following Stroke. Front Physiol 11:948.

Hanisch UK, Kettenmann H (2007) Microglia: active sensor and versatile effector cells in the normal and pathologic brain. Nat Neurosci 10:1387-1394.

Hu X, Li P, Guo Y, Wang H, Leak RK, Chen S, Gao Y, Chen J (2012) Microglia/macrophage polarization dynamics reveal novel mechanism of injury expansion after focal cerebral ischemia. Stroke 43:3063-3070.

Iadecola C (2017) The neurovascular unit coming of age: a journey through neurovascular coupling in health and disease. Neuron 96:17-42.

Jiang X, Andjelkovic AV, Zhu L, Yang T, Bennett MVL, Chen J, Keep RF, Shi Y (2018) Blood-brain barrier dysfunction and recovery after ischemic stroke. Prog Neurobiol 163-164:144-171.

Kettenmann H, Hanisch UK, Noda M, Verkhratsky A (2011) Physiology of microglia. Physiol Rev 91:461-553.

Kim KJ, Ramiro Diaz J, Iddings JA, Filosa JA (2016) Vasculo-neuronal coupling: retrograde vascular communication to brain neurons. J Neurosci 36:12624-12639.

Mallucci G, Peruzzotti-Jametti L, Bernstock JD, Pluchino S (2015) The role of immune cells, glia and neurons in white and gray matter pathology in multiple sclerosis. Prog Neurobiol 127-128:1-22.

Mishra A, Reynolds JP, Chen Y, Gourine AV, Rusakov DA, Attwell D (2016) Astrocytes mediate neurovascular signaling to capillary pericytes but not to arterioles. Nat Neurosci 19:1619-1627.

Miyake K, Takeo S, Kaijihara H (1993) Sustained decrease in brain regional blood flow after microsphere embolism in rats. Stroke 24:415-420.

Moskowitz MA, Lo EH, Iadecola C (2010) The science of stroke: mechanisms in search of treatments. Neuron 67:181-198.

Mustapha M, Nassir C, Aminuddin N, Safri AA, Ghazali MM (2019) Cerebral small vessel disease (CSVD)-lessons from the animal models. Front Physiol 10:1317.

Nishimura N, Rosidi NL, Iadecola C, Schaffer CB (2010) Limitations of collateral flow after occlusion of a single cortical penetrating arteriole. J Cereb Blood Flow Metab 30:1914-1927.

Patel AR, Ritzel R, McCullough LD, Liu F (2013) Microglia and ischemic stroke: a double-edged sword. Int J Physiol Pathophysiol Pharmacol 5:73-90.

Paxinos G, Franklin KB (2001) The Mouse Brain in Stereotaxic Coordinates. New York: Academic Press.

Prakash R, Carmichael ST (2015) Blood-brain barrier breakdown and neovascularization processes after stroke and traumatic brain injury. Curr Opin Neurol 28:556-564.

Qian B, Rudy RF, Cai T, Du R (2018) Cerebral artery diameter in inbred mice varies as a function of strain. Front Neuroanat 12:10.

Rapp JH, Pan XM, Neumann M, Hong M, Hollenbeck K, Liu J (2008) Microemboli composed of cholesterol crystals disrupt the blood-brain barrier and reduce cognition. Stroke 39:2354-2361.

Rapp JH, Pan XM, Yu B, Swanson RA, Higashida RT, Simpson P, Saloner D (2003) Cerebral ischemia and infarction from atheroemboli < 100 microm in Size. Stroke 34:1976-1980.

Rapp JH, Pan XM, Sharp FR, Shah DM, Wille GA, Velez PM, Troyer A, Higashida RT, Saloner D (2000) Atheroemboli to the brain: size threshold for causing acute neuronal cell death. J Vasc Surg 32:68-76.

Reeson P, Choi K, Brown CE (2018) VEGF signaling regulates the fate of obstructed capillaries in mouse cortex. Elife 7:e33670.

Shah FA, Li T, Kury LTA, Zeb A, Khatoon S, Liu G, Yang X, Liu F, Yao H, Khan AU, Koh PO, Jiang Y, Li S (2019) Pathological comparisons of the hippocampal changes in the transient and permanent middle cerebral artery occlusion rat models. Front Neurol 10:1178.

Shih AY, Hyacinth HI, Hartmann DA, van Veluw SJ (2018) Rodent models of cerebral microinfarct and microhemorrhage. Stroke 49:803-810.

Shih AY, Blinder P, Tsai PS, Friedman B, Stanley G, Lyden PD, Kleinfeld D (2013) The smallest stroke: occlusion of one penetrating vessel leads to infarction and a cognitive deficit. Nat Neurosci 16:55-63.

Shih AY, Fernandes HB, Choi FY, Kozoriz MG, Liu Y, Li P, Cowan CM, Klegeris A (2006) Policing the police: astrocytes modulate microglial activation. J Neurosci 26:3887-3888.

Shindo A, Ishikawa H, Ii Y, Niwa A, Tomimoto H (2020) Clinical features and experimental models of cerebral small vessel disease. Front Aging Neurosci 12:109.

Silasi G, She J, Boyd JD, Xue S, Murphy TH (2015) A mouse model of small-vessel disease that produces brain-wide-identified microocclusions and regionally selective neuronal injury. J Cereb Blood Flow Metab 35:734-738.

Smith EE, Schneider JA, Wardlaw JM, Greenberg SM (2012) Cerebral microinfarcts: the invisible lesions. Lancet Neurol 11:272-282.

Takano T, Tian GF, Peng W, Lou N, Libionka W, Han X, Nedergaard M (2006) Astrocyte-mediated control of cerebral blood flow. Nat Neurosci 9:260-267.

Taylor RA, Sansing LH (2013) Microglial responses after ischemic stroke and intracerebral hemorrhage. Clin Dev Immunol 2013:746068.

Tremblay M, Stevens B, Sierra A, Wake H, Bessis A, Nimmerjahn A (2011) The role of microglia in the healthy brain. J Neurosci 31:16064-16069.

Tsukada N, Katsumata M, Oki K, Minami K, Abe T, Takahashi S, Itoh Y, Suzuki N (2018) Diameter of fluorescent microspheres determines their distribution throughout the cortical watershed area in mice. Brain Res 1679:109-115.

van Veluw SJ, Shih AY, Smith EE, Chen C, Schneider JA, Wardlaw JM, Greenberg SM, Biessels GJ (2017) Detection, risk factors, and functional consequences of cerebral microinfarcts. Lancet Neurol 16:730-740.

Wang J, Xu D, Cui J, Wang S, She C, Wang H, Wu S, Zhang J, Zhu B, Bai W (2020) A new approach for examining the neurovascular structure with phalloidin and calcitonin gene-related peptide in the rat cranial dura mater. J Mol Histol 51:541-548.

Woodfin A, Voisin MB, Nourshargh S (2007) PECAM-1: a multi-functional molecule in inflammation and vascular biology. Arterioscler Thromb Vasc Biol 27:2514-2523.

Ye LX, An NC, Huang P, Li DH, Zheng ZL, Ji H, Li H, Chen DQ, Wu YQ, Xiao J, Xu K, Li XK, Zhang HY (2021) Exogenous platelet-derived growth factor improves neurovascular unit recovery after spinal cord injury. Neural Regen Res 16:765-771.

Zhang Q, Lan Y, He XF, Luo CM, Wang QM, Liang FY, Xu GQ, Pei Z (2015) Allopurinol protects against ischemic insults in a mouse model of cortical microinfarction. Brain Res 1622:361-367.

Zonta M, Angulo MC, Gobbo S, Rosengarten B, Hossmann KA, Pozzan T, Carmignoto G (2003) Neuron-to-astrocyte signaling is central to the dynamic control of brain microcirculation. Nat Neurosci 6:43-50.

C-Editor: Zhao M; S-Editors: Yu J, Li CH; L-Editors: Dawes EA, Song LP; T-Editor: Jia Y